Synthesis and characterization of Vanadium (V)-doped CZTS thin films by chemical spray pyrolysis method for solar cell applications

C. T. Illiyas[1] and K. C. Preetha[1,2,*]

[1] Department of Physics, Payyannur College, Affiliated to Kannur University, Payyannur, Kerala 670327, India
[2] Sree Narayana College, Varkala, Thiruvananthapuram, Kerala 695145, India

ABSTRACT

The Vanadium(V^{+5})-doped Cu_2ZnSnS_4(CZTS) thin films were synthesized by chemical spray pyrolysis technique. Structural properties were studied by X-ray Diffractometer (XRD) and Raman Spectrometer. Morphological and elemental compositions were studied by Scanning Electron Microscope with Energy-Dispersive X-ray analysis (SEM-EDX). Optical properties were determined by UV–VIS–NIR Spectrophotometer. The Electrical studies were carried out by Van der Pauw Ecopia HMS-3000 Hall Measurement System. The XRD patterns confirm the single-phase CZTS kesterite structure. The crystallite sizes were found to be decreasing with increasing the doping percentage. The Raman spectra further confirm the prominent kesterite structure of CZTS without any secondary phases. The SEM images exhibit non-uniform coral-shaped grain growth. The UV–VIS–NIR spectra show high absorption in the visible region and the band gaps were found to be increasing from 1.76 to 1.85 eV with increasing the doping percentage. The Hall measurements show high acceptor-type defects and high hole mobility for the V-doped CZTS. The pure and Vanadium-doped CZTS exhibit p-type conductivity, suitable for absorber layer of thin-film solar cells. The sample with high hole mobility and less absorption can be used as Hole Transport Layer (HTL) in Perovskite solar cells (PSCs).

1 Introduction

Serious research is being done in green energy technologies due to the environmental issues, the quickly depleting traditional energy resources and the need for renewable energy. Photovoltaic cells are excellent remote power choices to address a potential energy crisis [1]. Copper Indium Gallium Selenide (CIGS) photovoltaic systems had a record efficiency of 22.6% [2]. Due to the scarcity of Indium (In) and Tellurium (Te), as well as the toxicity of Cadmium (Cd) and Selenium (Se), thin-film solar cells like CIGS and Cadmium telluride (CdTe) have a restricted commercial manufacturing [3]. Copper Zinc Tin Sulphide

Address correspondence to E-mail: kcpreetha1990@gmail.com

🖄 Springer

(CZTS) solar cells were presented as the next generation of solar cells as a means of resolving these issues. The theoretical efficiency was stated to be 32%, and the efficiency of pure sulphide CZTS was reported to be over 10% [4]. As a result, vast area of research is to be done to increase the device efficiency of solar cells based on CZTS. Limitation that needs to be accomplished is caused bythe minority carrier lifetime of CZTS being lower than that of CIGS materials. If secondary phases are reduced, band tailing issues will be significantly improved, increasing the lifetime of minority carriers and reducing the efficiency gap between CIGS and kesterite CZTS. It is vital to use the doping technique, to manage the intrinsic defect so as to increase the efficiency of CZTS-based devices [4, 5].

CZTS has a direct band gap between 1.4 and 1.6 eV, a large absorption coefficient in the visible region ($> 10^4$ cm^{-1}) and p-type conductivity [6]. As per crystallography, CZTS quaternary semiconducting compounds primarily display two distinct cell structures, namely, kesterite and stannite as shown in Fig. 1, both have same structures but different Zn–Cu arrangements in their atomic positions in the crystal lattice [7]. Density and Melting point range of CZTS is 4.59 g/cm3 and 1260 K, respectively, suited for very high temperature preparations [8].

To comprehend the potential elements as dopants to improve solar cell efficiency, more research is necessary. Ag, Cd, Ge, etc., were utilized to enhance the device efficiency of the kesterite solar cell in comparison to the undoped CZTS [9]. Vanadium has not currently been examined as dopants. In order to improve the electrical properties of the kesterite absorber layer, the substitution of extrinsic elements into the kesterite matrix in varied ratios has become popular. The CIGS and CdTe device technologies are other sources of inspiration for this trend [9]. The extrinsic elements are used to minimize intrinsic defects and to provide facile dopants combined with the band gap engineering to boost the solar cell efficiency beyond 22% [4]. The preparation of CZTS thin films using a variety of deposition processes, including thermal deposition, pulsed laser deposition, electrodeposition, sol–gel spin coating, chemical bath deposition, and successive ionic layer absorption and reaction has been the subject of numerous investigations [7, 10, 11]. Out of these techniques, Chemical spray pyrolysis is one of the most efficient, easiest and economical uniform thin-film preparation technology.

2 Experimental methods

2.1 Materials used

All the reagents used were of analytical grade as obtained from Sigma-Aldrich 99.9% purity. Before the deposition, the cleaned glass slides were dipped in chromic acid (0.5 M) for 24 h and washed in deionized water. Then the substrate was degreased in acetone. Copper chloride ($CuCl_2.2H_2O$), Zinc acetate ($Zn(CH_3CO_2)_2.2H_2O$) and Tin chloride ($SnCl_2 2H_2O$) were used as cationic precursor solutions and Thiourea (CH_4N_2S) was used as anionic precursor solution. Sodium metavanadate ($NaVO_3$) was used for doping (V + 5).

2.2 Synthesis of CZTS thin film

The molarity of $CuCl_2.2H_2O$, Zn $(CH_3CO_2)_2.2H_2O$, $SnCl_2.2H_2O$ and CH_4N_2S were 0.04 M, 0.02 M, 0.02 M and 0.18 M, respectively. The concentration of the thiourea was taken more than stoichiometric ratio in order to compensate the evaporation of sulphur during air annealing. The cations were dissolved in deionized water, stirred for 30 min when the temperature reached 45 $^\circ$C, and thiourea was added and stirred for 1 h. The substrate temperature was kept constant at 250 $^\circ$C. The air flow rate and nozzle-to-substrate distance were kept fixed at 3 ml/min and 30 cm, respectively. The deposition was carried out for desired period of time and samples were allowed
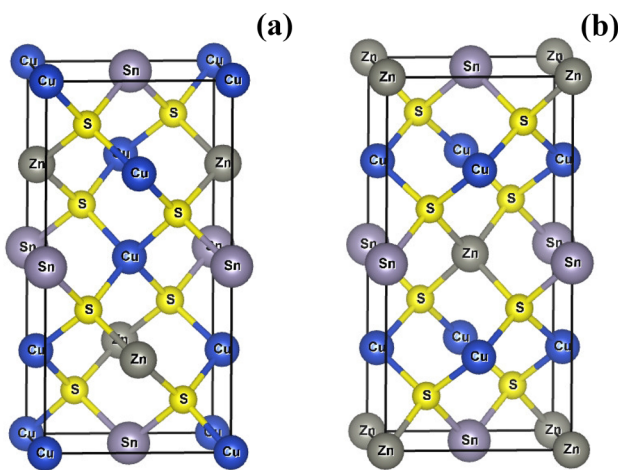

Fig. 1 **a** Kesterite-type CZTS **b** Stannite-type CZTS

to cool to room temperature. The Vanadium doping was varied as 1%, 2%, 3% and the samples were annealed at 300 °C for 30 min, named as CZTS, V1CZTS, V2CZTS and V3CZTS.

3 Characterization

The structural properties of CZTS thin films were carried out by X-ray diffraction (XRD-Rigaku miniflex 600) with CuKα radiation operated at an acceleration voltage of 40KV. Raman spectra were taken with Horiba Plus (Olympus BX43) spectrometer using 532 nm and 100 m Watt Diode Pump Solid State laser. The surface morphology and Elemental percentages of CZTS thin films were analysed by Scanning Electron Microscope with Energy-Dispersive X-ray spectroscope (SEM-EDX Joel 6390 LA/OXFORD XMX N). The optical absorption study was carried out in a wavelength range of 300–1200 nm using UV–VIS–NIR spectrophotometer (PerkinElmer Lambda 365). The thicknesses of all the samples were measured by Stylus profilometer (DEKTAK 6 M). The Electrical properties were carried out by Van der Pauw Ecopia HMS-3000 Hall Measurement System.

4 Result and discussion

4.1 Structural properties

Figure 2 exhibits the XRD results of all the samples. The major peaks at the planes (112), (220) and (312) correspond to the kesterite structure of CZTS (ICDD 26-0575) [12], which reveals that no subsequent binary or ternary phases were present during the formation of the distinctive tetragonal kesterite structure. To reduce the performance of the solar cell, the secondary phases will serve as charge barriers and recombination centres [5]. All of the undoped and V-doped samples are crystalline as seen by the sharpness of the peaks. The average sizes of crystallites (D) were calculated by Scherrer equation [13].

$$D = \frac{K\lambda}{\beta \cos(\theta)}, \tag{1}$$

where $K = 0.94$, λ is the wave length of characteristic CuKα X-ray incident radiation, represents the full width at half maxima (FWHM) of the diffraction peaks and stands for respective diffraction positions.

The crystallite sizes were found to be decreasing form 22 nm to 11 nm on increasing doping percentage of V. The peak positions of the intense peaks (112) and (220) were found to be shifting towards right as the doping percentage was increased and the orientation of the crystal was along the (112) plane. The dislocation densities (δ) and Microstrain (ε) of all the samples were calculated by Eqs. (2) and (3) [14]. Both ε and δ were found to be increasing with decreasing the crystallite size. The estimated structural parameters (D, δ and ε) are shown in Table 1.

$$\delta = \frac{1}{D^2} \tag{2}$$

$$\varepsilon = \frac{\beta \cos(\theta)}{4} \tag{3}$$

The lattice parameters were determined using the Bragg's Eq. (4) and the relation between miller indices (h,k,l) and inter-planar distance (d) for the kesterite structure [15].

$$\lambda = 2d \sin(\theta) \tag{4}$$

$$\frac{1}{d^2} = \frac{h^2 + k^2}{a^2} = \frac{l^2}{c^2}. \tag{5}$$

The estimated values of the lattice parameters 'a', 'c', 'c/a' and tetragonal cell volume were in good agreement with the previous experimental and theoretical reports [6]. It was observed that due to the shift in 2θ towards higher values, there is contraction in the cell volume of tetragonal CZTS as the doping percentage of V was increased, as shown in Table 2.

The phase purity of all the thin films were further investigated by the Raman spectra. Figure 3 shows the Raman spectra of the pure and Vanadium-doped CZTS thin films. A single intense Raman peak located at 327 cm^{-1} corresponds to A1 mode of vibration of the kesterite CZTS structure is observed in all films and is in well agreement with the value reported for bulk CZTS [16]. No additional peaks due to the phases such as CuS, ZnS, SnS, SnS2 and Cu2SnS3 have been observed [17]. These results ensure that the synthesized thin-film samples were the single-phase polycrystalline CZTS.

4.2 Morphological and elemental composition analysis

Morphology of the CZTS thin-film samples are displayed in Fig. 4. The films were inhomogeneous and
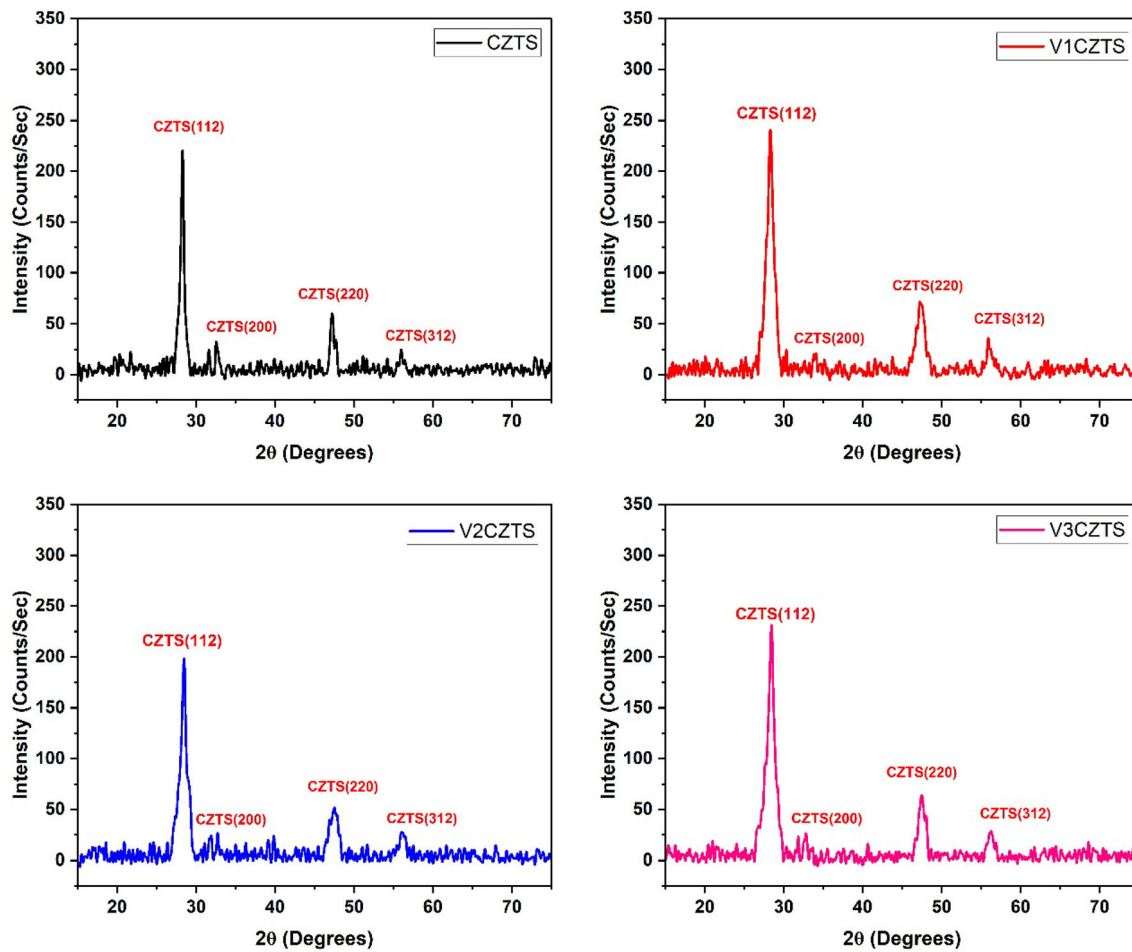
Fig. 2 XRD patterns of undoped and V-doped CZTS thin-film samples

Table 1 Structural parameters of CZTS and V-doped CZTS thin films

Sample name	Thickness (nm)	Miller indices (h,k,l)	2θ (degrees)	β (× 10^{-3} radians)	Avg. D (nm)	δ (× 10^{-3} Lines/nm²)	ε (10^{-3})
CZTS	2100	112	28.40	6.4	22	2.0	1.6
		220	47.33	7.2			
		312	56.02	7.5			
V1CZTS	2931	112	28.40	8.3	17	3.3	2.1
		220	47.35	8.9			
		312	55.94	11.2			
V2CZTS	2820	112	28.46	12.2	13	6.2	2.9
		220	47.55	15.4			
		312	56.15	11.3			
V3CZTS	2290	112	28.48	12.7	11	8.8	3.5
		220	47.44	16.7			
		312	56.20	15.4			

Table 2 The lattice parameters of pure and Vanadium-doped CZTS thin films

Sl. No	Sample name	Lattice parameters			
		a (Å)	c (Å)	c/a	Volume (Å^3)
1	CZTS	5.43	10.92	2.01	322
2	V1CZTS	5.43	10.93	2.02	322
3	V2CZTS	5.40	10.95	2.03	319
4	V3CZTS	5.42	10.88	2.01	319

porous, and look like coral shape. It was found that the grain size enlarges with the incorporation of V in the kesterite CZTS. The porous shapes will increase the surface area of the CZTS grains. The EDX spectrum of undoped and V-doped CZTS thin films was composed of Cu, Zn, Sn, S and in well agreement with the stoichiometric values of kesterite CZTS. The presence of Vanadium is also visible in the EDX

spectrum as shown in Fig. 5. The obtained atomic percentage in EDX analysis is shown in Table 3. The percentage of V in the doped samples are less than 1% which may be due to the inhomogeneity of the surface of the scanning area of the samples.

4.3 Optoelectronic properties

The absorption spectra of undoped and V-doped samples as displayed in Fig. 6a, b indicate that maximum absorption is in the visible region of the solar spectrum. The absorption peak in the UV region was found to be decreasing with the incorporation of Vanadium in CZTS.

The band gaps were calculated from Tauc's relation between absorption coefficient (α), and the energy of incident photon (hv) [18].

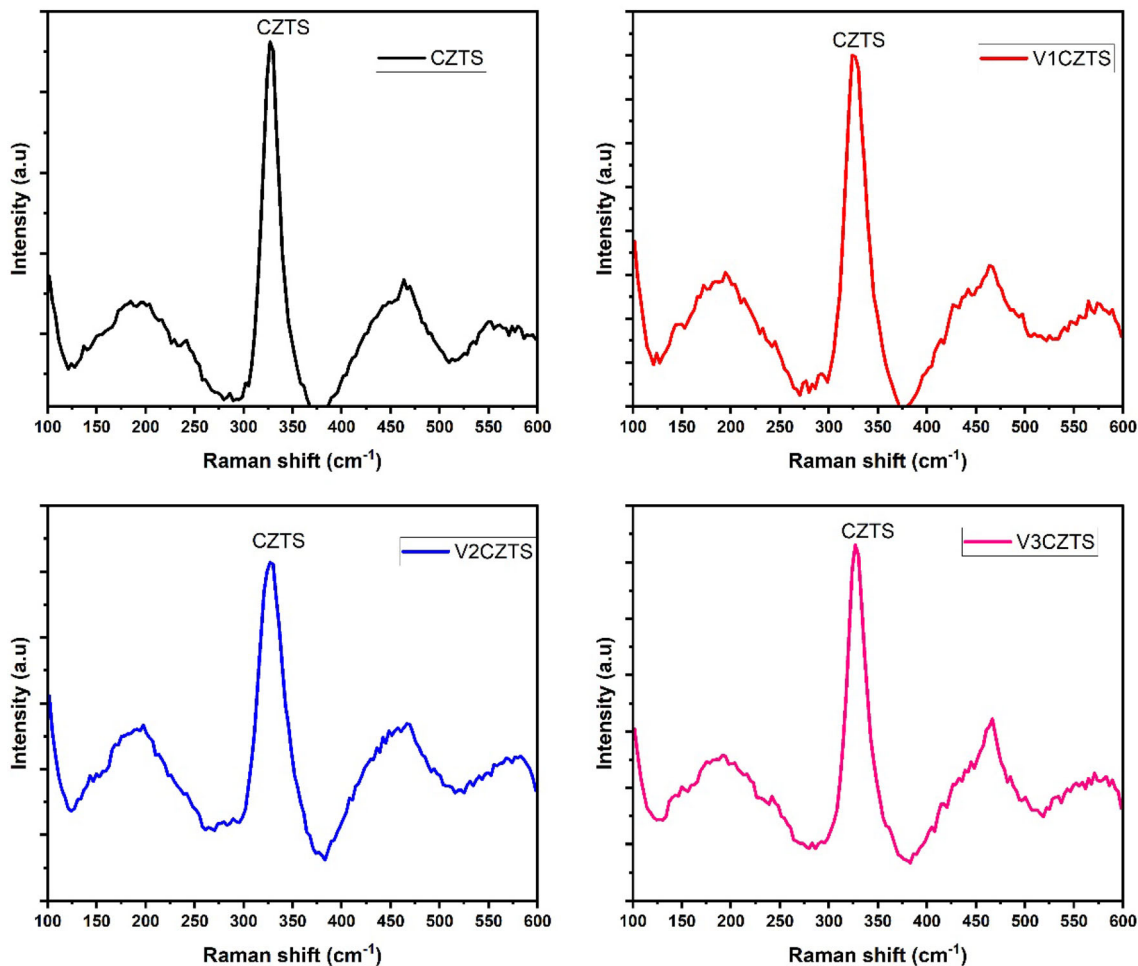$$\alpha h v = A\left(h v - E_g\right)^\gamma, \tag{6}$$

Fig. 3 Raman spectra of CZTS thin-film samples

Fig. 4 a SEM image of undoped CZTS **b** SEM image of V1CZTS **c** SEM image of V2CZTS and **d** SEM image of V3CZTS
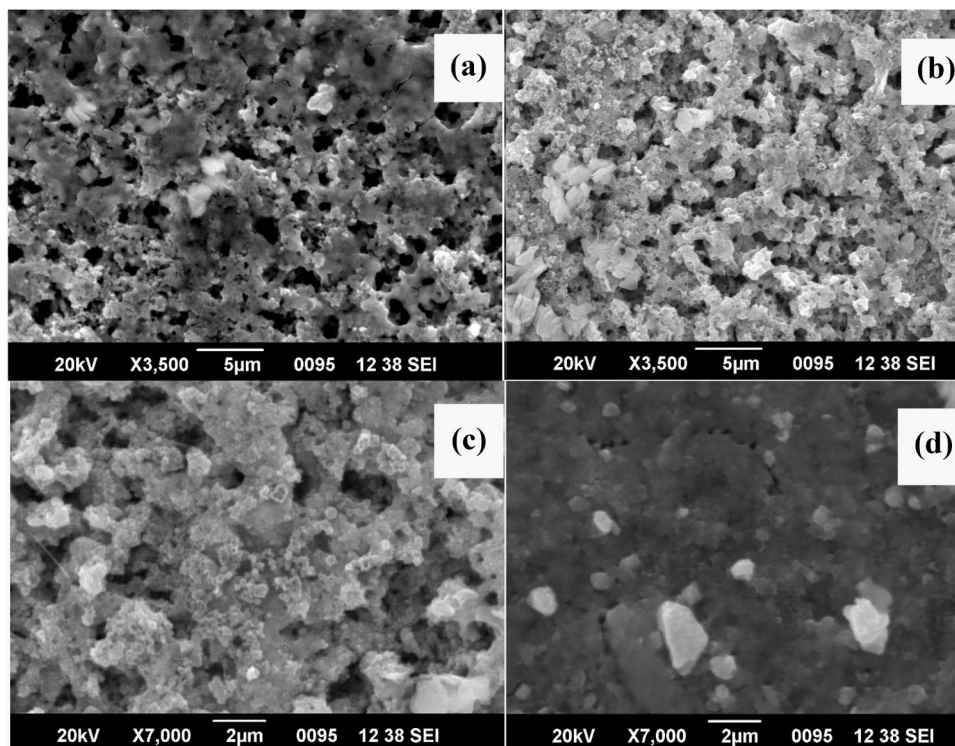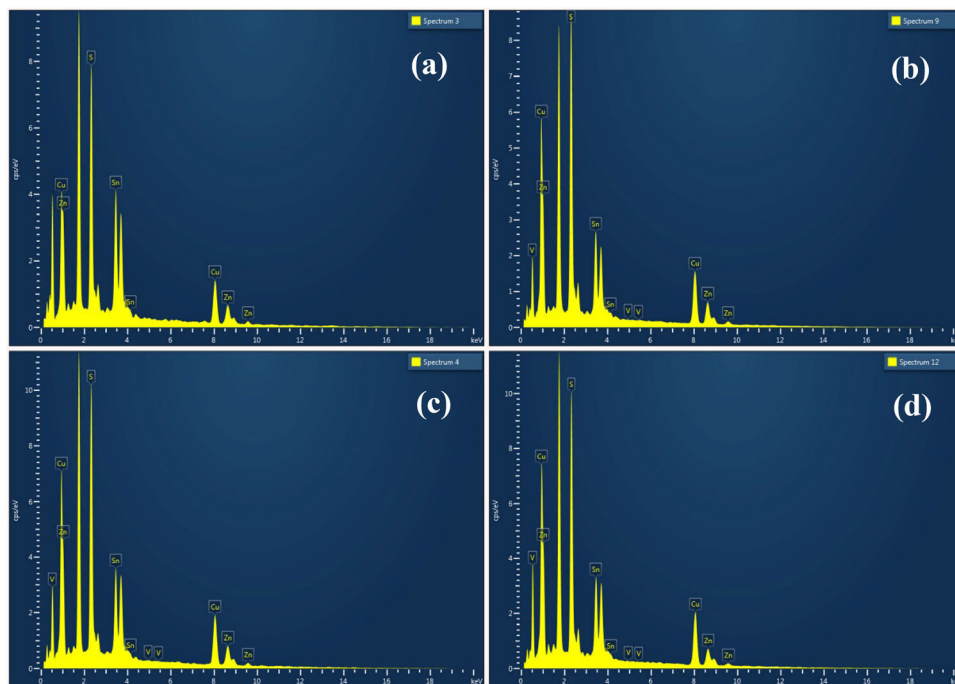

Fig. 5 a EDX spectrum of CZTS **b** EDX spectrum of V1CZTS **c** EDX spectrum of V2CZTS and **d** EDX spectrum of V3CZTS

where 'A' is a constant, 'E_g' is the band gap and the parameter 'γ' depends on the type of electronic transition with values 1/2, 2, 3/2 and 3 for allowed direct, allowed indirect, forbidden direct and forbidden indirect transitions, respectively. Since the kesterite CZTS structure has direct allowed transition, 1/2 was used. The optical band gap is determined by extrapolating the linear part of the data curves of $(\alpha h)^2$ at the intercept on the photon energy axis. The estimated band gaps (E_g) are 1.76 eV, 1.78

Table 3 Elemental percentage of CZTS samples from EDX analysis

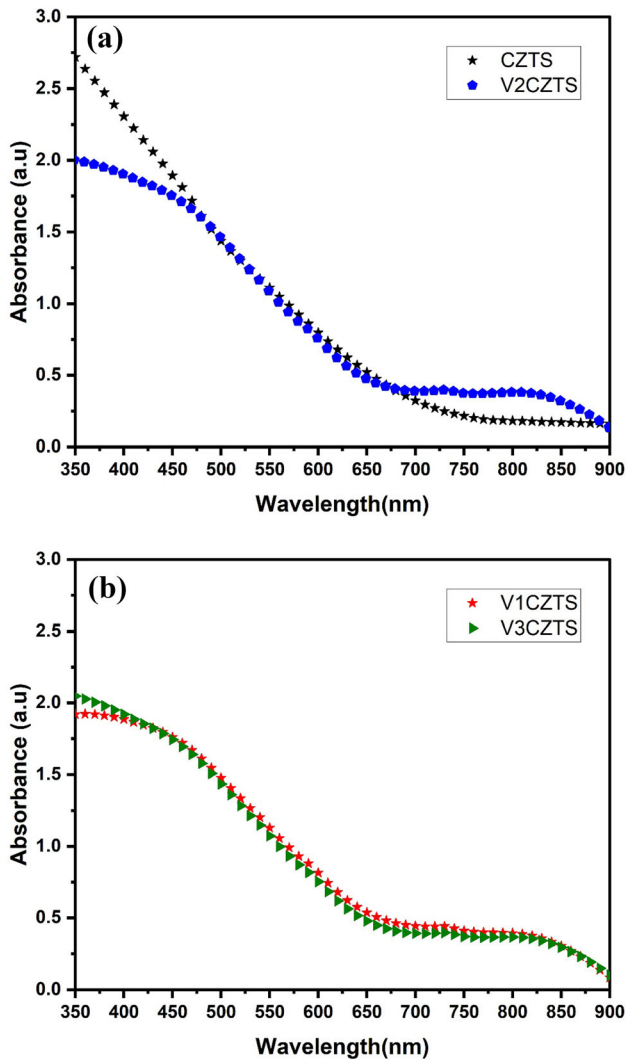| Sample name	Atomic %				
	Cu	Zn	Sn	S	V
CZTS	25.77	13.38	14.98	45.00	0.00
V1CZTS	26.95	12.35	13.96	46.51	0.23
V2CZTS	26.86	13.73	13.35	45.73	0.33
V3CZTS	27.46	13.35	14.24	44.60	0.34

Fig. 6 a Absorption spectra of CZTS and V2CZTS. **b** Absorption spectra of V1CZTS and V3CZTS

eV, 1.80 eV and 1.85 eV for CZTS, V1CZTS, V2CZTS and V3CZTS, respectively, as shown in Fig. 7. The band gap was found to be increasing with increasing the doping from 1 to 3%, which is consistent with the

structural analysis. The variation of crystallite size and band gap with doping percentage of V is shown in Fig. 8.

The transmission spectra of the undoped and doped samples are shown in Fig. 9, the transmittance is very low in the visible region. The percentage of Transmittance significantly varies as it goes to the NIR region.

The absorption coefficients of all the samples were in the range of 10^4 cm^{-1} and are depicted in Fig. 10. It is found that the values of α of Vanadium-doped samples were less than that of undoped CZTS sample.

The Urbach edge, which reflects the transition between the valance band and the conduction band tail states, can be used to represent the quality of the material and it was calculated using the following formula [19].

$$\alpha = \alpha_0 \exp\left(\frac{h\nu}{E_u}\right), \tag{7}$$

where E_u represents the Urbach energy and α_0 is constant. E_u can be estimated from the reciprocal of the straight-line slopes of the variation of 'ln α' with '$h\nu$' as shown in Fig. 11. The obtained values of E_u lie in the range of 256 meV to 409 meV. The lower values of E_u represent the high quality of the thin films.

The carrier concentration (p), hole mobility (μ_p), resistivity (ρ), conductivity (σ) and type of conductivity were determined by Van der Pauw Ecopia HMS-3000 Hall Measurement System and are shown in Table 4. All the samples show high carrier concentrations of order of 10^{18}–10^{20} cm^{-3}. The pure and V-doped samples confirm the p-type conductivity. In kesterite CZTS one anion is surrounded by tetrahedrally coordinated four cations (2Cu, 1Zn, 1Sn) as illustrated in Fig. 12. The intrinsic defect formation energy of Cu$_{Zn}$ antisite (Cu replaces Zn) is lower than all other acceptor and donor defects which has higher hole population density, and is responsible for p-type conductivity of CZTS crystals [20]. The donor defects Sn$_{Zn}$ (Sn replaces Zn) will contribute two electrons to the crystal which will compensate the holes generated and reduce the hole concentration. It is evident from Table 4 that the extrinsic impurity Vanadium also acts as donor defects in the CZTS crystal, decreasing the hole population. The sample V2CZTS has hole concentration greater than V1CZTS due to Zn-rich atomic percentage than others. All values of conductivity lie in the semiconductor range. The
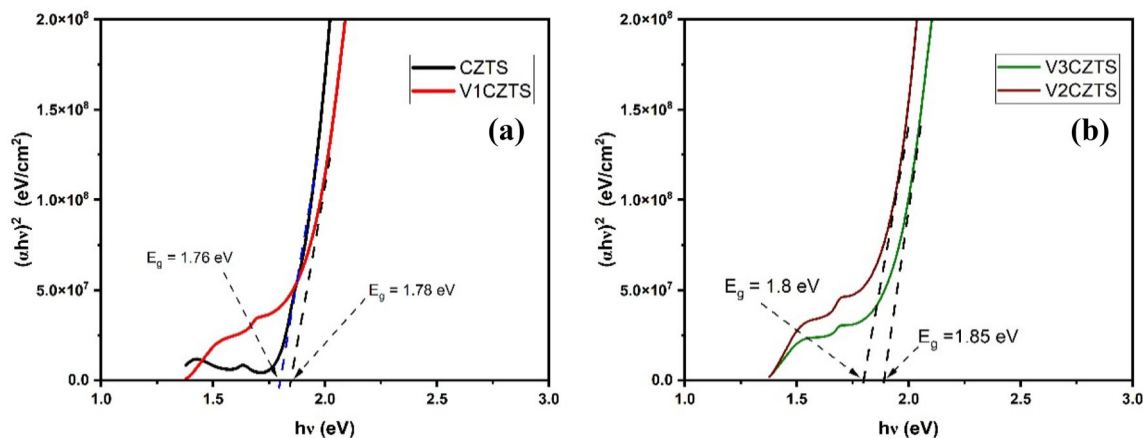
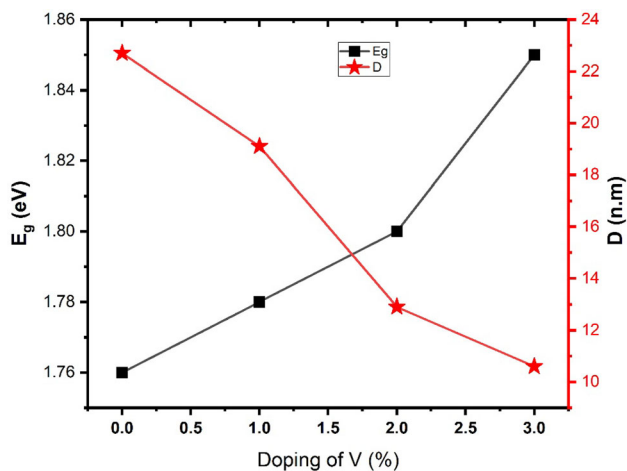**Fig. 7** Tauc plot of Vanadium-Doped and Undoped CZTS thin-film samples

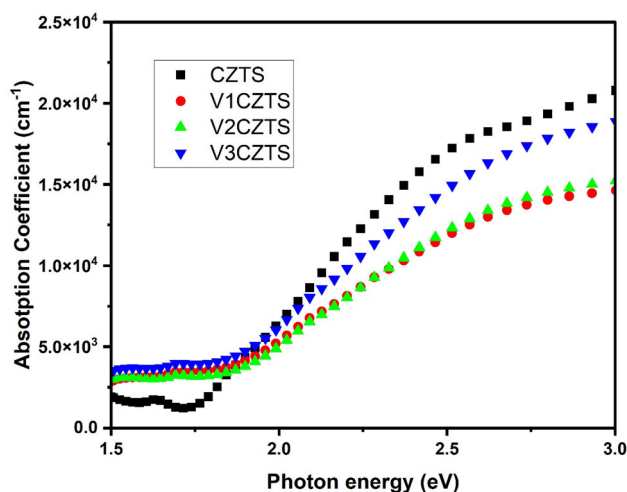**Fig. 8** Variation of crystallite size and band gap with V doping

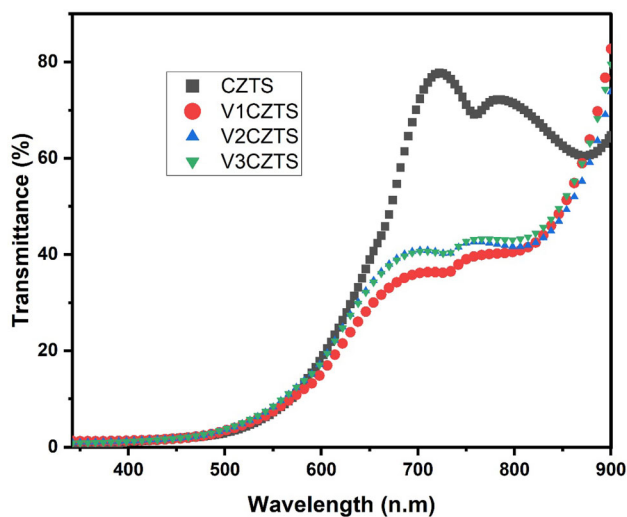**Fig. 10** Absorption Coefficient of CZTS and V-doped CZTS thin films

Fig. 9 Transmission spectrum of CZTS thin-film samples

conductivity of the 1% doped sample was found to be less than that of the undoped sample, but increases with doping percentage of Vanadium, which implies that the conductivity can be controlled by suitable amount of Vanadium doping. The value of μ_p is found to be increasing with decreasing the hole concentration which is consistent with earlier reports [4]. The values of μ_p can be increased with doping percentage of V as shown in Fig. 13. For perovskite solar cell the Hole Transport layer (HTL) must have high hole mobility, therefore the sample V3CZTS is suitable HTL candidate for perovskite solar cells (PSCs). The sample with high absorption coefficient is a promising absorber layer for CZTS-based thin-film solar cells.
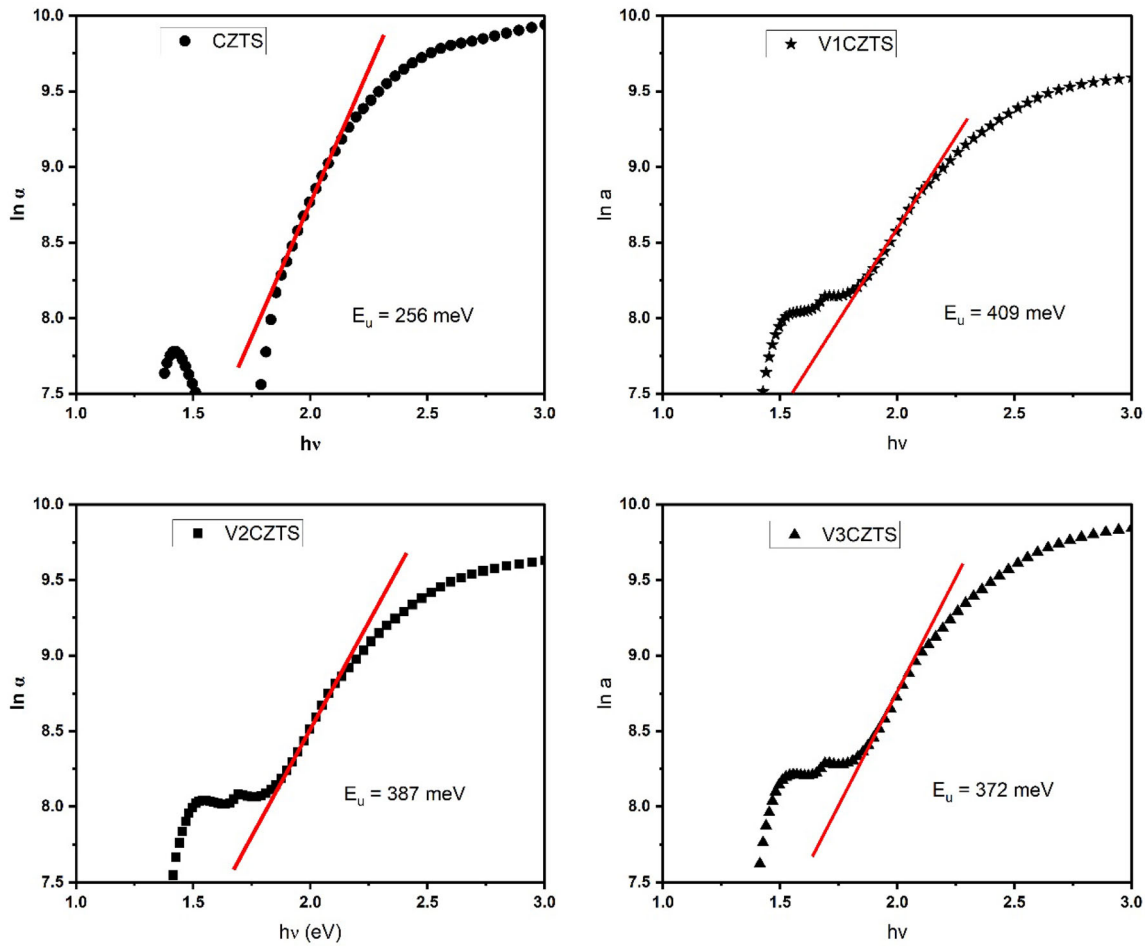
Fig. 11 Urbach plots of undoped and V-doped CZTS thin films

Table 4 Hall measurement parameters of V-doped CZTS samples

Film name	p (cm^{-3})	μ_p (cm^2/vs)	σ (Ω^{-1} cm^{-1})	Type
CZTS	1.75×10^{20}	0.554	15.50	p-type
V1CZTS	9.04×10^{18}	1.274	1.85	p-type
V2CZTS	1.32×10^{20}	0.353	7.47	p-type
V3CZTS	7.47×10^{18}	8.091	9.68	p-type

Fig. 12 Tetrahedrally coordinated Sulphur atom

5 Conclusions

The XRD patterns confirmed the single-phase polycrystalline CZTS with kesterite structure. The crystallite sizes were found to be decreasing with doping percentage of vanadium (+ 5). The Raman spectra analysis further confirmed the prominent tetragonal kesterite structure 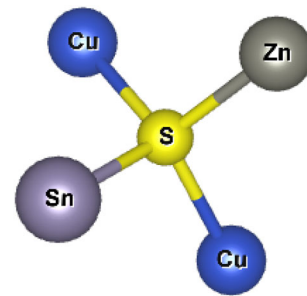of CZTS. The UV–VIS–NIR spectra showed high absorption in the visible region and the band gaps were found to be increasing from 1.76 to 1.85 eV with increasing the doping percentage of V. The SEM images exhibited porous and coral-shaped grain growth. The Hall measurements showed the pure CZTS and Vanadium-doped CZTS as p-type semiconductor, suitable absorber layer for thin-film solar cells and vanadium-doped samples with high
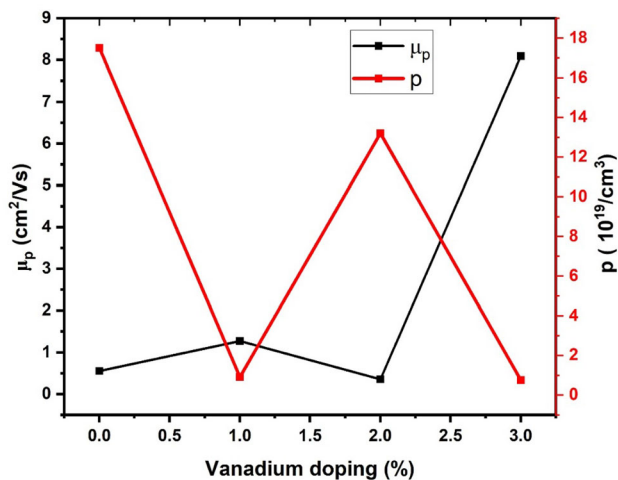
Fig. 13 Variation of mobility and hole concentration with vanadium doping

hole mobility and less absorption can be used as Hole transport layer in Perovskite solar cells.

Author contributions

All authorscontributed to the study conception and design. Materials preparation, datacollection and analysis were performed by CTI. The first draft of themanuscript was written by CTI and KCP. All authors commented onprevious version of the manuscript. All authors read and approved the finalmanuscript.

Data availability

All data generated oranalysed during this study are included in this article.

Code availability

All data generated or analysed during this study are included in this article.

Declarations

Conflict of interest The authors declarethat they have no known competing financial interests or per-sonalrelationships that could have appeared to influence the work reported in thispaper.

Ethical approval Not Applicable.

References

1. S.A. Vanalakar, P.S. Patil, J.H. Kim, Sol. Energy Mater. Sol. Cells. **182**, 204 (2018)

2. S. Saha, Int. J. Photoenergy **2020**, 1 (2020)

3. A.S. Nazligul, M. Wang, K.L. Choy, Sustainability. **12**, 5138 (2020)

4. S. Lie, M. Guc, V. Tunuguntla, V. Izquierdo-Roca, S. Siebentritt, L.H. Wong, J. Mater. Chem. A **10**, 9137 (2022)

5. M.V. Jyothirmai, H. Saini, N. Park, R. Thapa, Sci. Rep. **9**, 15983 (2019)

6. B.L. Guo, Y.H. Chen, X.J. Liu, W.C. Liu, A.D. Li, AIP Adv. **4**, 097115 (2014)

7. X. Song, X. Ji, M. Li (2014) https://www.hindawi.com/journals/ijp/2014/613173/

8. M. Ravindiran, C. Praveenkumar, Renew. Sustain. Energy Rev. **94**, 317 (2018)

9. Y.E. Romanyuk, S.G. Haass, S. Giraldo, M. Placidi, D. Tiwari, D.J. Fermin, X. Hao, H. Xin, T. Schnabel, M. Kauk-Kuusik, P. Pistor, S. Lie, L.H. Wong, J. Phys. Energy. **1**, 044004 (2019)

10. S. Harikengaram, M. Robinson, A. Chellamani, Chalcogenide Lett. **16**, 89 (2019)

11. S. Rao, A. Morankar, H. Verma, P. Goswami, J. Appl. Chem. **2016**, 1 (2016)

12. S. Patel, J. Gohel, Phys. Astron. Int. J **1**, 1 (2017)

13. R. Govindaraj, V. Asokan, Indian J. Pure Appl. Phys. (IJPAP). **52**, 620 (2015)

14. J. Henry, K. Mohanraj, G. Sivakumar, Optik. **141**, 139 (2017)

15. N.P. Huse, A.S. Dive, S.V. Mahajan, R. Sharma, J. Mater. Sci.: Mater. Electron. **29**, 5649 (2018)

16. M.-Y. Yeh, P.-H. Lei, S.-H. Lin, C.-D. Yang, Materials. **9**, 526 (2016)

17. K. Diwate, K. Mohite, M. Shinde, S. Rondiya, A. Pawbake, A. Date, H. Pathan, S. Jadkar, Energy Procedia. **110**, 180 (2017)

18. K.C. Preetha, T.L. Remadevi, Mater. Sci. Semiconduct. Process. **24**, 179 (2014)

19. M. Mathew, K.C. Preetha, Pramana. **95**, 174 (2021)

20. S. Chen, L.-W. Wang, A. Walsh, X.G. Gong, S.-H. Wei, Appl. Phys. Lett. **101**, 223901 (2012)